

# Data Fusion of PRISMA Satellite Imagery for Asbestos-containing Materials: An Application on Balangero's Mine Site (Italy)

Giuseppe Bonifazi<sup>1</sup><sup>a</sup>, Giuseppe Capobianco<sup>1</sup><sup>b</sup>, Riccardo Gasbarrone<sup>1</sup><sup>c</sup>, Silvia Serranti<sup>1</sup><sup>d</sup>, Sergio Bellagamba<sup>2</sup><sup>e</sup> and Daniele Taddei<sup>1,\*</sup><sup>f</sup>

<sup>1</sup>DICMA, Department of Chemical Engineering, Materials and Environment, Sapienza - University of Rome, via Eudossiana 18, 00184, Italy

<sup>2</sup>INAIL - Italian Workers' Compensation Authority, Research Division, DIT - Department for Technological Innovations and Security Equipment, Products and Human Settlements, via R. Ferruzzi 38/40, Rome, Italy

**Keywords:** PRISMA, Imaging Spectroscopy, Classification, Asbestos, Asbestos-containing Materials (ACMs).

**Abstract:** In the last few decades, the procedure for identifying, classifying and mapping the asbestos-containing materials (ACMs), and contaminated areas, is considered one of the most important aspects for the purpose of remediation. This task, carried out by skilled workers, can be very long and difficult to perform, and it can also increase the risk of inhalation of asbestos fibers. The identification and characterization of areas contaminated by asbestos using remote sensing techniques represent a valid alternative to census methods, traditionally based on visual inspection of surfaces and *in situ* sampling to be analyzed later in the laboratory. The aim of this work was to explore the possibilities of using machine learning techniques to identify possible asbestos-contaminated areas and ACMs by using PRISMA satellite imagery in areas where chrysotile was once extracted, processed and used in asbestos-containing products (ACPs). The study area is located in the Balangero's asbestos mine site. More in detail, Principal Component Analysis (PCA) was performed on a Visible, Near-InfraRed and Short-Wave InfraRed (VNIR-SWIR) PRISMA image to reduce data dimensionality and used as an exploratory analysis tool. Classification And Regression Trees (CART) technique was finally utilized to test a classification of six predetermined classes on the panchromatic image.

## 1 INTRODUCTION

In many countries, asbestos contaminated areas are still a relevant issue. Asbestos was widely used during the 20th century thanks to its important physical and mechanical characteristics.

There is not a group of minerals that, from a mineralogical point of view, goes under the name 'asbestos', but there are various mineral types that can be distinguished based on their crystallographic and chemical characteristics. According to the European applicable legal references, the general term 'asbestos' is used to identify six naturally occurring

silicate minerals belonging to the serpentine (Chrysotile) and amphibole (Amosite, Crocidolite, Tremolite, Anthophyllite and Actinolite). They can be found in several different crystalline forms, but only the fibrous forms are classified as asbestos (Council of the European Union, 2003). Based on numerous epidemiological studies carried out since the 1960s and proving the carcinogenic nature of these fibers, all the asbestos minerals have been classified as carcinogens by the International Agency for Research on Cancer (IARC) (Paglietti et al., 2016). Many countries like Italy, have thus banned the production, importation, processing and distribution of Asbestos-Containing Products (ACPs)

<sup>a</sup> <https://orcid.org/0000-0001-6935-2686>

<sup>b</sup> <https://orcid.org/0000-0003-1914-7275>

<sup>c</sup> <https://orcid.org/0000-0003-4739-1582>

<sup>d</sup> <https://orcid.org/0000-0003-2435-5212>

<sup>e</sup> <https://orcid.org/0000-0002-4295-0704>

<sup>f</sup> <https://orcid.org/0000-0002-2814-8459>

Eudossiana 18, 00184 Rome, Italy, Tel:+39-3471866206

(i.e. roofing sealant, pipe lagging, duct tape, furnace cement and glue for flooring, etc.) and Asbestos-Containing Materials (ACMs) (i.e. corrugated cement sheets, flat cement sheets, etc.) and have recommended action plans for the mapping and safe removal of asbestos from public and private buildings and remediation of highly contaminated areas (Paglietti et al., 2016). The procedure to identify, classify and map ACMs and contaminated areas is considered one of the most important aspects for the purpose of remediation; this procedure performed by skilled workers can be very long and difficult to perform, and it can also increase the risk of inhalation of asbestos fibers. Scientific literature reports many studies on the utilization of remote sensing techniques to map asbestos in anthropic and natural environment, using different approaches (Amano et al., 2008; Chen et al. 2012; Aplin et al. 2008; Blaschke, 2010) as hyperspectral remote sensing (Frassy et al., 2014; Marino et al. 2001; Massarelli et al. 2017). Several studies have also explored the abilities to identify ACMs by HyperSpectral Imaging (HSI) proximal sensing in Short-Wave InfraRed (SWIR) (Bonifazi et al., 2018; Bonifazi et al. 2019; Serranti et al. 2019).

Aim of this work was to explore the possibilities of using machine learning techniques to identify possible asbestos-contaminated areas and ACMs by using PRISMA (Hyperspectral PRecursor of the Application Mission) satellite imagery (ASI, 2009) in areas where chrysotile was once extracted, processed, and used in ACPs. Principal Component Analysis (PCA) was performed on a Visible and Near-InfraRed - Short-Wave InfraRed (VNIR-SWIR) PRISMA image to reduce data dimensionality and used as an exploratory analysis tool. Classification And Regression Trees (CART) technique was used to test a classification of six classes (i.e. 'ACM', 'Urban Area', 'Anthropogenic vegetation', 'Natural vegetation', 'Water', 'Balangero's mine'), predetermined on the panchromatic image. The classification was performed on a novel dataset, where the panchromatic image was fused with the PCA scores resulting from the application of PCA on the VNIR-SWIR dataset. The data fusion strategy selected was mid-level (Figure 1). According to this procedure the features extracted from the different blocks are concatenated to build a single array which is then processed by the desired chemometric technique (Biancolillo et al. 2014).

## 2 MATERIALS AND METHODS

The studied areas are located near Turin, in the Piedmont region (Northern Italy), the former

Balangero's and Corio's asbestos mine site (Figure 2 and Figure 3).

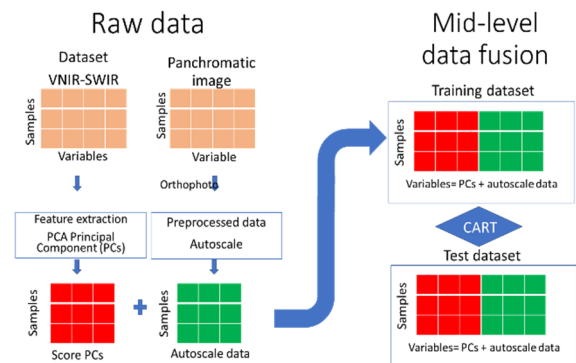


Figure 1: Scheme of the data-fusion and classification approach adopted.

Figure 2 shows an asbestos mining (2a) characterized by the presence of building roofs containing asbestos and a rural area (2b) with building roofs where asbestos presence was not detected.



(a)



(b)

Figure 2: Balangero's asbestos mining site with building roofs containing asbestos (a) and rural areas with building roofs without asbestos (b).



(a)



(b)

Figure 3: Portion of the underwater asbestos open-pit mine with presence of natural vegetation (a) and urban area with the presence of an abandoned industrial site where roofs contain asbestos (b).

Figure 3a shows another portion of asbestos mine with presence of natural vegetation. Figure 3b shows and urban area with the presence of an abandoned industrial site where building roofs contain asbestos. The datasets corresponding to Figure 2 were used as calibration set, while the datasets corresponding to Figure 3 were utilized as validation set.

### 2.1 Data Handling and Processing

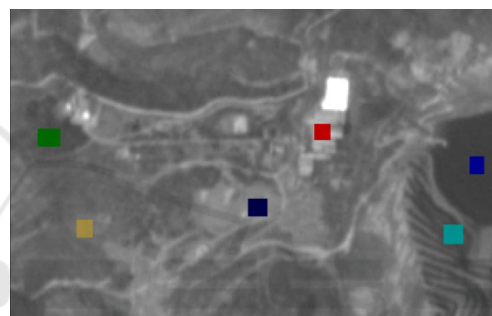
The PRISMA equipment is made up of an imaging spectrometer, able of acquiring VNIR (Visible and Near-InfraRed) and SWIR (Short-Wave InfraRed) images (~ 250 bands), with a spatial resolution of 30 m on a swath of 30 km, and a panchromatic camera with spatial resolution of 5 m. The spectral resolution

is about 12 nm in the spectral range of 400-2500 nm, that are VNIR and SWIR regions (ASI, 2009).

The PRISMA VNIR-SWIR hyperspectral image and the panchromatic image datasets were imported into the MATLAB® environment (R2021a, Version 9.10, The Mathworks, Inc.). The details of utilized dataset are shown in Table 1.

Table 1: Dataset sizes.

		Area 1	Area 2
Raw data VNIR-SWIR	Training dataset	193*304*23 (Figure 1a)	213*224*234 (Figure 1 b)
	Prediction dataset	125*191*234 (Figure 2a)	240*190*234 (Figure 2b)
Raw data panchromatic image	Training dataset	193*304*1 (Figure 1a)	213*224*1 (Figure 1 b)
	Test dataset	125*191*1 (Figure 2a)	240*190*1 (Figure 2b)



- ACM
- Natural vegetation
- Water
- Balangero's Mines
- Anthropogenic vegetation
- Urban area

Figure 4: Region of Interests (ROIs) selected on the panchromatic image.

The imported data were analyzed using the PLS\_Toolbox (Version 8.2 Eigenvector Research, Inc.) (Wise et al., 2006) and Statistics and Machine Learning Toolbox. The PLS\_Toolbox was used to pre-process data and for performing the Principal Component Analysis (PCA), while Statistics and Machine Learning Toolbox was utilized for setting up the Classification And Regression Trees (CART).

### 2.2 Class Setting

From a small part of the panchromatic image, depicting near a half of the open-pit mine and its surrounding, six Region of Interests (ROIs) were selected and the following classes were set: ACM, Urban Area, Anthropogenic vegetation, Natural vegetation, Water and Balangero's mine (Figure 4).

The above-mentioned classes were then selected according to surface truth to the ground. In 'ACM' was included Asbestos Containing Materials (i.e. Eternit corrugated roofing). In 'Urban Area' were included areas characterized by urban morphology. In 'Anthropogenic vegetation' were selected areas with cultivated crops. In 'Natural vegetation' were included areas with woods and sparse trees patterns. While, in 'Water' class was included the underwater open-pit mine area. Finally, 'Balangero's mine' class was chosen selecting barren areas near the open-pit mine. The class set of the panchromatic image was then transferred to the VNIR-SWIR dataset.

### 2.3 Data Pre-processing

Spectral data preprocessing is a necessary step in order to reduce detector noise, to eliminate the spectral nonuniformity due to the illumination, scattering phenomena and the influence of the changing environmental conditions. Data pre-treatment is also addressed to better solve the spectra information by enhancing differences among the classes. To choose the right pre-processing algorithms, different pre-processing algorithms were tested among those widely adopted (Rinnan & Engelsen, 2009). The algorithms combination which gave the best data decomposition of the class scores were selected. The adopted pre-processing combination was spatial Median Filter (MF), Standard Normal Variate (SNV), Gap-Segment (GS) 1<sup>st</sup> Derivative and Multiway Center (MC).

### 2.4 Principal Component Analysis

The Principal Component Analysis (PCA) is a well-known data exploratory method, widely adopted to HSI datasets, that gives the possibility to have an overview of complex multivariate data. PCA allows to reduce the dimensionality of a data matrix containing multiple interrelated variables, while retaining as much as possible of the variation present in the data set (Bro et al., 2014). In this case, PCA was carried out to detect outliers and choose the data to built-up the classifiers by reducing the dimensionality of the dataset. The PCA was performed on the VNIR-SWIR dataset. Six PCs were chosen. The scores of the performed PCA were then concatenated with the panchromatic image.

### 2.5 Classification and Regression Trees (CART)

Classification And Regression Trees (CART), a non-parametric statistical technique, was used to classify

the six classes on the panchromatic image fused with the PCA scores (Shao et al. 2012). Classification And Regression Trees (CART), a non-parametric statistical technique, was used to classify the six classes on the panchromatic image fused with the PCA scores. CART classification algorithm, developed by Breiman et al. (1984), allows to build a decision tree based on Gini's impurity index as splitting criterion. In classification and regression problems, CART algorithm produces a decision tree describing a response varying as a function of multiple explanatory variables. A tree hierarchy is produced by the subdivision process.

In the tree hierarchy, the observation subsets are represented by the nodes, while the leaves are the final nodes. A binary model, formulated in each node, is responsible for the subdivision process. In each node, all the samples satisfying the model are clustered in a sub-group, while the remaining nodes are assigned to another subgroup. The classification process therefore follows a path along the tree from the root towards a final leaf. This process can be synthesized in three steps. In the 1<sup>st</sup> step of CART analysis, the binary split procedure allows to build the maximum tree by finding the best split which maximizes the splitting criterion. Usually, overfitting can occur when the maximum tree is overgrown closely describing the used training set. To correct the overfitted model a pruning process occurs in the 2<sup>nd</sup> step. The pruned model results in multiple less complex tree, that are derived from the maximum tree. In the 3<sup>rd</sup> step, finally, a cross-validation process helps to select the optimal tree (Deconinck et al. 2006).

The main advantage of CART algorithm relies on the fact of being nonparametric. Moreover, it can be used in combination with other prediction algorithms and by combining both testing with a test data and cross-validation thus enabling to more precisely measure the quality of the model fitting.

### 2.6 Classification Performance Metrics

The performance evaluation of the classification methods was carried out in terms of prediction maps, that is false colour images representing the classification and in terms of the statistical parameters: Sensitivity and Specificity (Ballabio & Todeschini, 2009). In more detail, the Sensitivity represents the ability of determined classifier to correctly recognize samples belonging to a specified class and is defined by Equation (1). On the other hand, Specificity relates to the model ability to

correctly reject samples belonging to all the other classes as defined by Equation (2).

$$Sensitivity = \frac{TP}{TP + FN} \tag{1}$$

$$Specificity = \frac{TN}{TN + FP} \tag{2}$$

TP are the total number of True Positive, FN the total number of False Negative, TN the total number of True Negative and FP the total number of False Positive. Sensitivity and Specificity were calculated according to the number of correctly or not correctly assigned pixel to each defined class, with reference to calibration (CAL), cross-validation (CV) and to the prediction of the validation set (PRED).

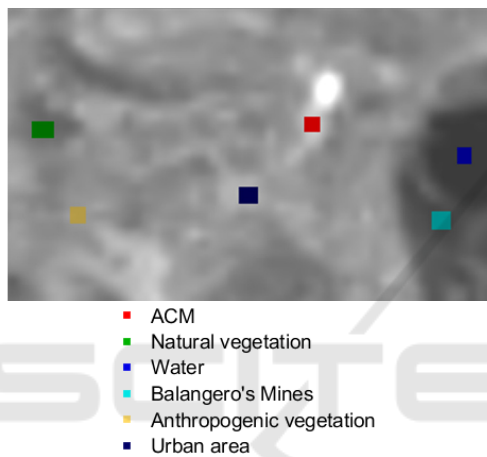


Figure 5: Region of Interests (ROIs) transferred from the panchromatic image to the VNIR-SWIR dataset.

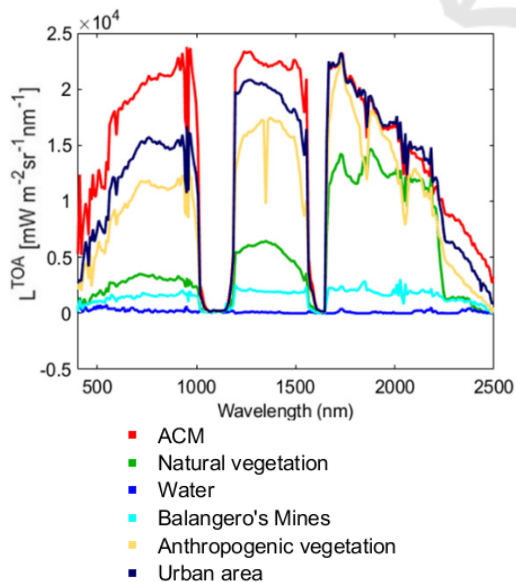


Figure 6: Raw spectra of the six classes. ( $L^{TOA}$ : Top of Atmosphere radiance).

### 3 RESULTS AND DISCUSSION

The six Region of Interests (ROIs) selected on the panchromatic image and transferred to the VNIR-SWIR dataset (Figure 5) and corresponding mean spectra are shown in Figure 6. The average spectra of the six classes show significant spectral differences but are also very noisy. For this reason, in order to reduce the noise and emphasize the spectral variation (as already explained in the Chapter 2.3), the data were pre-processed as shown in Figure 7.

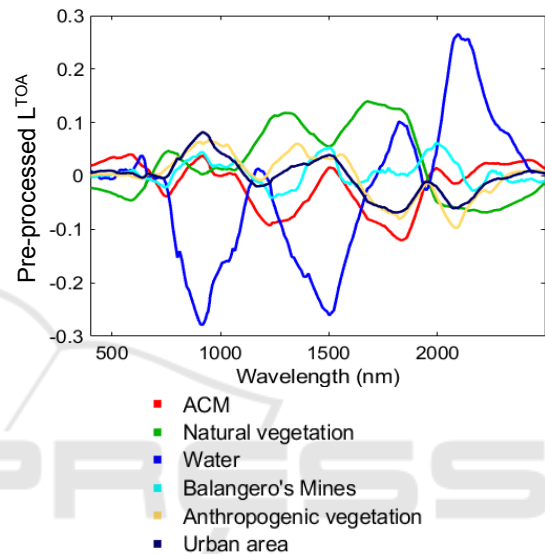


Figure 7: Pre-processed spectra averaged for the six classes. The adopted pre-processing combination is spatial Median Filter (MF), Standard Normal Variate (SNV), Gap-Segment (GS) 1st Derivative and Multiway Center (MC).

After data preprocessing, a PCA model was created (Figure 8). PCA model allows to capture 99.69% of the total variance with six principal components. In detail, the PCA score plot of PC1 and PC3 shows 6 separated clusters corresponding to the 6 different classes considered (i.e. ‘ACM’, ‘Urban Area’, ‘Anthropogenic vegetation’, ‘Natural vegetation’, ‘Water’ and ‘Balangero’s mine’). The positive space of scores on PC3 is mainly influenced by ‘Balangero’s Mines’ spectra. The negative space of scores on PC1 is mainly influenced by water of Balangero’s lake. The combination of the positive value of scores PC1 and negative value of scores on PC3 allows the separation of ‘Urban area’, ‘Anthropogenic’ and ‘Natural vegetation’. Finally, the ACM class is separated from the other classes by the combination of negative PC1 and positive PC3 values.

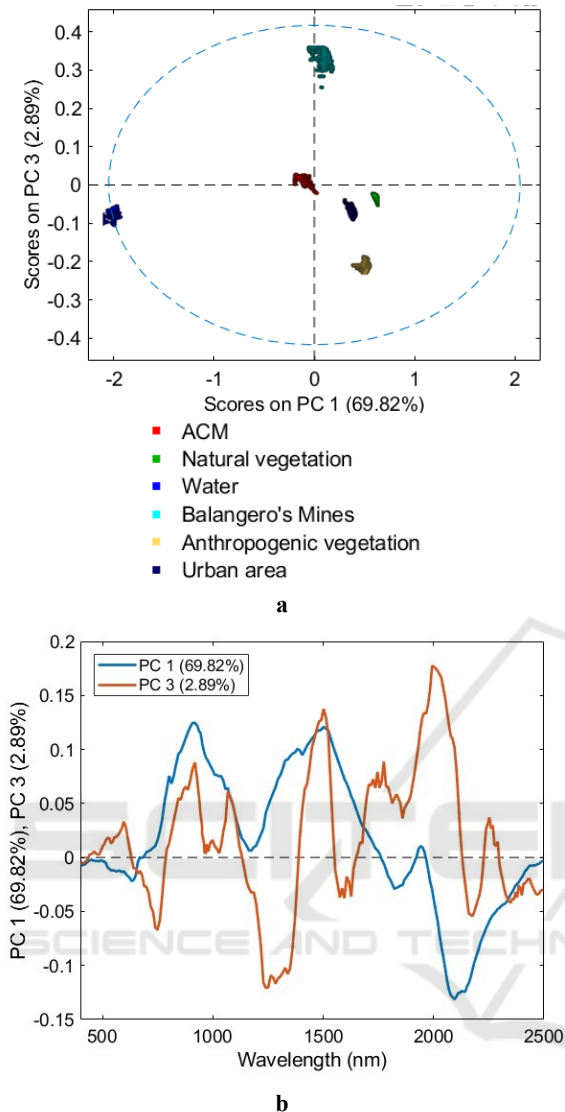


Figure 8: PCA scores plot (a) and loadings plot (b) of the first and third PCs.

The negative space of scores on PC1 is mainly influenced by water of Balangero's lake. The combination of the positive value of scores PC1 and negative value of scores on PC3 allows the separation of 'Urban area', 'Anthropogenic' and 'Natural vegetation'. Finally, the ACM class is separated from the other classes by the combination of negative PC1 and positive PC3 values.

Starting from the good separation obtained, this PCA model was used for the data reduction of PRISMA hyperspectral datasets. The PCA-reduced datasets were concatenated to the corresponding panchromatic images as shown in the example reported in Figure 9. In detail, the concatenated procedure allows to combine chemical information

coming from VNIR-SWIR range with the shapes and contours of the topographical details obtained from the panchromatic image.

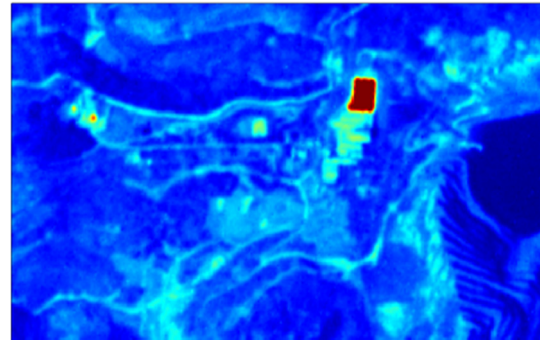


Figure 9: False color image of the novel dataset, resulting from the fusion of VNIR-SWIR PCA scores and the panchromatic of the studied area.

Starting from this new data set, the classes for the calibration dataset were set as shown in Figure 10. The calibration set was then created and utilized to build the CART model.

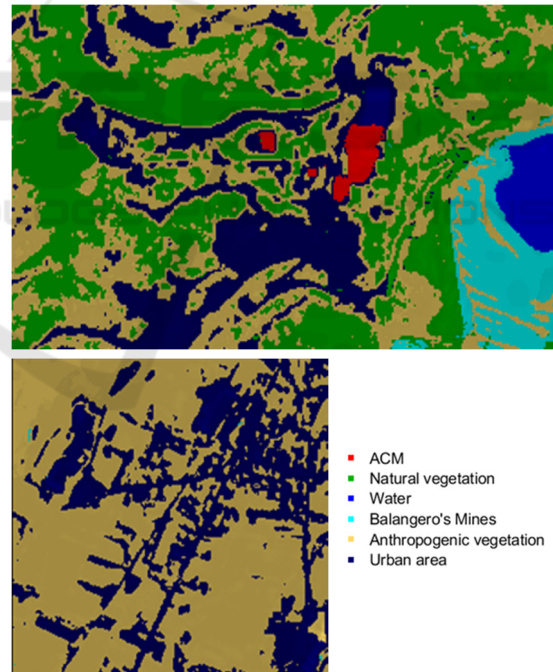


Figure 10: Class map of the Training set.

The results in terms of Sensitivity and Specificity (Table 2) confirm the good performance of the model, with values ranging from 0.816 ('ACM' class) to 0.980 ('Water' class) and 0.979 ('Anthropogenic vegetation' class) to 1.00 ('Water class'), respectively, both in calibration and cross-validation.

Table 2: results in terms of Sensitivity and Specificity.

Class	Sens. (Cal)	Spec. (Cal)	Sens. (CV)	Spec. (CV)
ACM	1,000	1,000	0.816	0.999
Anthropogenic vegetation	1,000	1,000	0.981	0.979
Balangero's Mines	1,000	1,000	0.946	0.997
Natural vegetation	1,000	1,000	0.962	0.992
Urban area	1,000	1,000	0.963	0.988
Water	1,000	1,000	0.980	1.000

The CART prediction map of the validation set is reported in Figure 11, whereas the performance metrics of the classification model applied to the validation set are shown in Table 3. The results in terms of prediction images (Figure 11) are in agreement with those achieved in the calibration phase. By analyzing the performance metric parameters reported in Table 3, despite a slight decrease in sensitivity in the identification of ACM roofs, is clear that the identification of the main structures with asbestos is correct, confirming the success of the proposed test.

#### 4 CONCLUSIONS

In this paper, a novel approach was developed and implemented to identify ACM from "Urban Area", Anthropogenic and natural vegetation", "Water" and "Balangero's mine".

PRISMA satellite hyperspectral images were elaborated through multivariate statistical analysis in order to extract the chemical features of the classes. Subsequently, the PRISMA hyperspectral data, reduced by PCA, were concatenated with the panchromatic image in order to combine chemical information with the shapes and contours of the topographical details. Afterwards, starting from the fused dataset, a CART classification model was developed in order to recognize the roofing containing asbestos from other objects on the images.

The adopted procedure proved to have a significant discriminating capacity in terms of sensitivity and specificity enabling the possibility to use this approach for more extended areas.

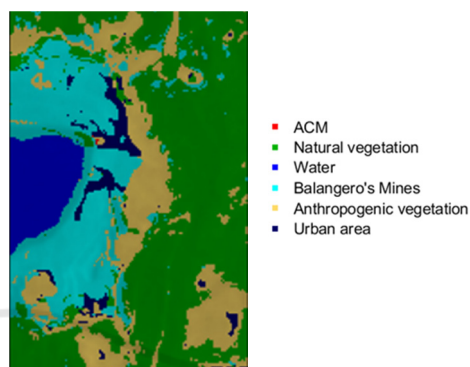
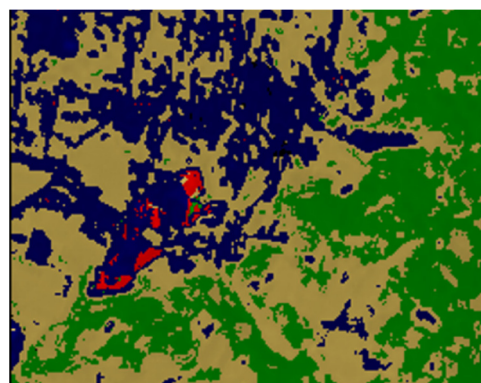


Figure 11: CART prediction map.

Table 3: Performance metrics of CART classification in prediction calculated on the test set.

Class	Sens. (Pred)	Spec. (Pred)
ACM	0.756	0.997
Anthropogenic vegetation	0.993	0.981
Balangero's Mines	0.999	0.993
Natural vegetation	0.937	0.997
Urban area	0.980	0.994
Water	1.000	1.000

The possibility of a systematic and integrated use of PRISMA image combined with machine learning tools for ACMs identification, proved to be a complementary method for a faster identification and mapping of contaminated areas, with less risk of exposure for operators and the possibility to perform a fast and reliable survey of ACPs by remote sensing.

The fulfilment of the previous mentioned goals could produce positive environmental impacts, as well as big economic benefits related to the lower identifying and mapping costs.

## ACKNOWLEDGEMENTS

The study was developed in the framework of INAIL (Italian National Institute for Insurance against Accidents at Work) project: *BRIC ID 60/2 - Valutazione e comparazione dei livelli di informazione ottenibili da remoto con sensoristica ottica innovativa per l'identificazione di MCA in diversi contesti del territorio nazionale; confronto dei dati ottenuti con risultati analitici acquisiti in laboratorio. Definizione di tecniche di campionamento ed analisi per il monitoraggio della presenza di erionite.*

## REFERENCES

- Amano, Y., Takagi, N and Getz, AFH. (2008). *A study on the classification of urban region using hyper-spectrum data at AVIRIS. In: Geoscience and Remote Sensing Symposium, 2008. IGARSS 2008. IEEE International.*, Boston, MA, USA: IEEE, pp. 687-690.
- Aplin, P. & Smith, G.M. (2008). *Advances in Object Based Image Classification. The International Archives of the Photogrammetry, Remote Sensing and Spatial Information Sciences*, Beijing, Vol.37, 725-728. [http://www.isprs.org/proceedings/XXXVII/congress/7\\_pdf/4\\_WG-VII-4/45.pdf](http://www.isprs.org/proceedings/XXXVII/congress/7_pdf/4_WG-VII-4/45.pdf)
- Ballabio, D. & Todeschini, R. (2009). *Multivariate classification for qualitative analysis. Infrared spectroscopy for food quality analysis and control*, 83, e102.
- Biancolillo, A., Bucci, R., Magri, A. L., Magri, A. D., & Marini, F. (2014). *Data-fusion for multiplatform characterization of an Italian craft beer aimed at its authentication. Analytica chimica acta*, 820, 23-31.
- Blaschke, T. (2010). *Object-based Image Analysis for Remote Sensing. ISPRS Journal of Photogrammetry and Remote Sensing*, 65, 2-16.)
- Bonifazi, G., Capobianco, G., & Serranti, S. (2018). *Asbestos containing materials detection and classification by the use of hyperspectral imaging. Journal of hazardous materials*, 344, 981-993.
- Bonifazi, G., Capobianco, G., & Serranti, S. (2018). *Asbestos containing materials detection and classification by the use of hyperspectral imaging. Journal of hazardous materials*, 344, 981-993.
- Bonifazi, G., Capobianco, G., & Serranti, S. (2019). *Hyperspectral imaging and hierarchical PLS-DA applied to asbestos recognition in construction and demolition waste. Applied Sciences*, 9(21), 4587.
- Breiman, L., Friedman, J., Olshen, R., & Stone, C. (1984). *Cart. Classification and Regression Trees; Wadsworth and Brooks/Cole: Monterey, CA, USA.*
- Bro, R., & Smilde, A. K. (2014). *Principal component analysis. Analytical methods*, 6(9), 2812-2831.
- Chen, Z., Ning, X. and Zhang, J. (2012). *Urban Land Cover Classification Based on WorldView-2 Image Data. IEEE International Symposium on Geomatics for Integrated Water Resource Management, Lanzhou*, 19-21 October 2012, 1-5.
- Deconinck, E., Zhang, M. H., Coomans, D., & Vander Heyden, Y. (2006). *Classification tree models for the prediction of blood-brain barrier passage of drugs. Journal of chemical information and modeling*, 46(3), 1410-1419.
- Directive 2003/18/EC of the European Parliament and of the Council of 27 March 2003 amending Council Directive 83/477/EEC on the protection of workers from the risks related to exposure to asbestos at work.
- Frassy, F., Marchesi, A., Candiani, G., Rusmini, Marco., Maianti, P., Marchesi, A., Rota Nodari, F., Della Via, G., Albonico, C., Gianinetto, Marco. (2014) "Mapping Asbestos Cement Roofing with Hyperspectral Remote Sensing over a Large Mountain Region of the Italian Western Alps," *Sensors*, vol. 14, no. 9, pp. 1590015913, doi: 10.3390/s140915900.
- Marino, C. M., Panigada, C. and Busetto, L. (2001) *Airborne hyperspectral remote sensing applications in urban areas: asbestos concrete sheeting identification and mapping*, IEEE/ISPRS Joint Workshop on Remote Sensing and Data Fusion over Urban Areas (Cat. No.01EX482), pp. 212216, doi: 10.1109/DFUA.2001.985882.
- Massarelli, C., Matarrese, R., Uricchio, V. F., Muolo, M. R., Laterza M. & Ernesto L. (2017) *Detection of asbestos containing materials in agroecosystem by the use of airborne hyperspectral CASI1500 sensor including the limited use of two UAVs equipped with RGB cameras. International Journal of Remote Sensing*, 38:810, 21352149, DOI: 10.1080/01431161.2016.1226528
- Paglietti, F., Malinconico, S., della Staffa, B. C., Bellagamba, S., & De Simone, P. (2016). *Classification and management of asbestos-containing waste: European legislation and the Italian experience. Waste management*, 50, 130-150.
- Rinnan, Å., Van Den Berg, F., & Engelsen, S. B. (2009). *Review of the most common pre-processing techniques for near-infrared spectra. TrAC Trends in Analytical Chemistry*, 28(10), 1201-1222.
- Serranti, S., Bonifazi, G., Capobianco, G., Malinconico, S., & Paglietti, F. (2019, May). *Hyperspectral imaging applied to asbestos containing materials detection: specimen preparation and handling. In Advanced Environmental, Chemical, and Biological Sensing Technologies XV (Vol. 11007, p. 110070S). International Society for Optics and Photonics.*
- The PRISMA mission (PDF). ASI. 4 September 2009. Archived from the original (PDF) on 4 October 2013. Retrieved 23 August 2013.
- Wise, B. M., Gallagher, N. B., Bro, R., Shaver, J. M., Windig, W., & Koch, R. S. (2006). *Chemometrics tutorial for PLS Toolbox and Solo. Eigenvector Research, Inc*, 3905, 102-159.
- Shao, Y., Lunetta, R. S. (2012) *Comparison of support vector machine, neural network, and CART algorithms for the landcover classification using limited training data points. ISPRS Journal of Photogrammetry and Remote Sensing, Volume 70, Pages 7887.*